Explosion characteristics of hydrous bio-ethanol in oxygen-enriched air

Xu, C., Wu, S., Li, Y., Chu, S. & Wang, C.

Original citation & hyperlink:
Xu, C, Wu, S, Li, Y, Chu, S & Wang, C 2020, 'Explosion characteristics of hydrous bio-ethanol in oxygen-enriched air', Fuel, vol. 271, 117604.
https://dx.doi.org/10.1016/j.fuel.2020.117604

DOI 10.1016/j.fuel.2020.117604
ISSN 0016-2361

Publisher: Elsevier

Explosion characteristics of hydrous bio-ethanol in oxygen-enriched air

Cangsu Xu [a], Siyuan Wu[a], Yanfei Li[b], Shuhua Chu[a], Chongming Wang[bc*]

[a] *College of Energy Engineering, Zhejiang University, Hangzhou, China, 310027*

[b] *State Key Laboratory of Automotive Safety and Energy, Tsinghua University, Beijing, China, 100084*

[c] *School of Engineering, Coventry University, Coventry, UK, CV1 5FB*

**Corresponding author email address: ac8174@coventry.ac.uk (Chongming Wang)*

Abstract

Hydrous bio-ethanol is a promising alternative fuel, which consumes less energy during the production than anhydrous bio-ethanol. However, hydrous bio-ethanol features a slow burning rate, leading to low combustion stability, or even misfire especially at a high water content. Preliminary research shows that oxygen-enriched combustion (oxy-combustion) effectively solves the slow burning rate issue. However, oxy-combustion might increase the potential explosion hazard. Therefore, it is essential to study explosion characteristics of hydrous bio-ethanol oxy-combustion before its application in practical engines. In this paper, an explosion characteristic study was carried out in a constant volume combustion chamber (CVCC). Hydrous bio-ethanol with 20 vol% water (E80W20) was selected. E80W20 is selected considering the tradeoff between production energy saving and burn rate. The boundary conditions for the experiments are initial pressures of 1-4 bar, initial temperatures of 358-418 K, air with the oxygen concentrations of 21-25% and equivalence ratios of 0.7-1.4. Explosion parameters such as explosion pressure, maximum rate of pressure rise, deflagration index, and combustion duration were analyzed. Results show that both the explosion pressure and maximum rate of pressure rise linearly increase with the initial pressure. Deflagration index increases linearly with the oxygen concentration, but it is not sensitive to initial temperature. In most cases, the deflagration index is lower than 20 MPa·m/s, revealing that E80W20 is relatively safe when it is combusted with air with a 23% oxygen content. This work paves the way for the application of hydrous bio-ethanol oxy-combustion in practical engines.

Keywords: Hydrous bio-ethanol, oxy-combustion, deflagration index, safety

Symbols

P_{max}	Explosion pressure (bar)
P	Pressure (bar)
P_0	Initial pressure (bar)
$(dP/dt)_{max}$	Maximum rate of pressure rise (bar /s)
dP/dt	Pressure rise rate (bar /s)
K_G	Deflagration index (MPa*m/s)
t	Time after ignition (s)
t_c	Combustion duration (s)
T_0	Initial temperature (K)
Q	Total released heat (kJ)
k_u	Specific heat ratio
ϕ	Equivalence ratio
a	Intercept of explosion pressure function
b	Pressure sensitivity coefficient of explosion pressure function
c	Intercept of maximum rate of pressure rise function
d	Pressure sensitivity coefficient of maximum rate of pressure rise function
e	Intercept of deflagration index function
k	Pressure sensitivity coefficient of deflagration index function

1. Introduction

To satisfy the increasingly stringent emission regulations and requirements of the sustainable development strategy, the development of efficient and clean internal combustion engines has become the focus of powertrain researchers [1]. Apart from advanced engines, biofuel is effective in reducing greenhouse gas emissions. Currently, the most widely used biofuel is bio-ethanol. The first-generation bio-ethanol is produced from crops and sugar canes, and the second-generation is produced from low-value lignocellulosic biomass such as woody crops and agricultural residues. Pure bio-ethanol can be used in specially designed engines, or it can be blended with gasoline and used in engines with some modifications. As a gasoline alternative, bio-ethanol has preferred physiochemical properties. Apart from high octane number, bio-ethanol has a higher latent heat of vaporization than gasoline (904 kJ/kg for ethanol against 350 kJ/kg for gasoline), leading to a higher cooling effect in direct injection engines [2-4]. Gasoline containing anhydrous ethanol is proved to reduce the deposit formation in the fuel injection system [5-7]. Hydrous bio-ethanol weakens the reduction effects of CO and HC emissions, but it further reduces NO_x emissions [2,3]. Moreover, recent studies show that fuel with a high octane sensitivity, defined as the difference between research octane number and motor octane number, has a better anti-knock tendency [8-10].

However, anhydrous bio-ethanol production is highly energy-intensive, especially when removing water through distillation and dehydration processes [11]. Generally, after the completion of the fermentation process, ethanol concentration in the ethanol-water solution is approximately 12 vol%. Distillation is often employed for increasing the purity of ethanol from 12 vol% to 80 vol%. The energy consumption during this process is almost linear: for every 10 vol% increase in purity, the consumption is 0.31 MJ/L, corresponding to a 1.15% ethanol lower heating value (21.3 MJ/L). However, from 80%

to the azeotropic point (96.5 vol%), the energy requirement exponentially increases [12]. If engines can use hydrous ethanol directly, the energy consumption during ethanol fuel production can be reduced rapidly, leading to significant energy saving during the production phase.

Some studies have been conducted on the combustion of hydrous ethanol [11,13-15], and it has been found that the one issue of burning hydrous ethanol is a low burning rate. Compared with anhydrous ethanol, there is a 15-40% reduction in burning rate for hydrous ethanol with a 20 vol% - 40 vol% water content, which leads to poor thermal efficiency and even misfires [15,16]. Oxy-combustion is a feasible way to solve the problem. Moreover, oxy-combustion is an important zero-emission technology. When pure oxygen is used as the oxidant for combustion, the exhaust gas only contains CO_2 and H_2O, making the separation of CO_2 technically easier [17,18]. However, the use of oxy-enriched air also implies potential safety problems, as an increase in the oxygen concentration will greatly increase the reactivity and flammability range of combustible mixtures [19], which means that there is an explosion hazard of the combustible mixtures. Thus, it is very essential to know the explosion characteristics of hydrous ethanol in oxygen-enriched air before it is applied in practical engines.

Explosion and combustion invovles the similar phenomenon, however, explosion features a much faster burning rate and a pressure rise. According to BS EN 1839:2017 [20], the combustion of a flammable mixture with pressure build-up of 5% more than the initial pressure is regarded as an explosion. De Smedt et al. [21] also pointed out that a test showing a pressure rise of 7% or more is called an explosion. What's more, combustion is usually used in the study of IC engines, whereas explosion is usually used in the study of combustion-related safety. Recently, fundamental research of ethanol combustion and explosion has been carried out. Rahman et al. [22] examined the combustion

characteristics of hydrous ethanol in a constant volume combustion chamber (CVCC). They found a qualitative relationship between the water content and the combustion duration. They also simulated the laminar burning velocity of hydrous ethanol by using existing chemical kinetic mechanisms. Yi Fei [23] studied the oxy-combustion of low concentration ethanol solutions and he analyzed the effects of total oxidizer flow rate and ethanol concentration on blow-off limit. Mitu and Brandes et al. [24] studied explosion characteristics of ethanol in two closed spherical vessels under different initial conditions. They found that the explosion pressure and the maximum rate of pressure rise correlated linearly with the initial pressure. Li et al. [25] studied explosion characteristics of five alcohol-air mixtures over wide ranges of initial temperatures and pressures. They found the difference in explosion behaviours of these mixtures shrank with the increase of initial pressure. In addition, the explosion parameters of three primary alcohols gave similar values at the lean equivalence ratio end, but the difference was gradually enlarged at the rich equivalence ratio end. Mitu et al. [26] investigated explosion parameters of ethanol with various ethanol concentrations in the presence of diverse diluents and proposed the effect of the diluent types and dilution ratios on the explosion characteristics.

However, to the best of authors' knowledge, no data is available for the explosion characteristics of oxy-combustion of hydrous ethanol. Therefore, in this paper, the hydrous ethanol was studied in a CVCC at the initial temperatures of 358-418 K, initial pressures of 1-4 bar, oxygen concentrations of 21-25 % and equivalence ratios of 0.7-1.4. Explosion parameters such as explosion pressure P_{max}, maximum rate of pressure rise $(dP/dt)_{max}$, deflagration index K_G and combustion duration t_c are employed as quantitative indicators for the explosion characteristics.

2. Experimental setup

Fig. 1 schematically presents the layout of the experimental system, which is mainly composed of a CVCC, a heating device, a high-speed Schlieren photography system, an electrode ignition system and a data acquisition system.

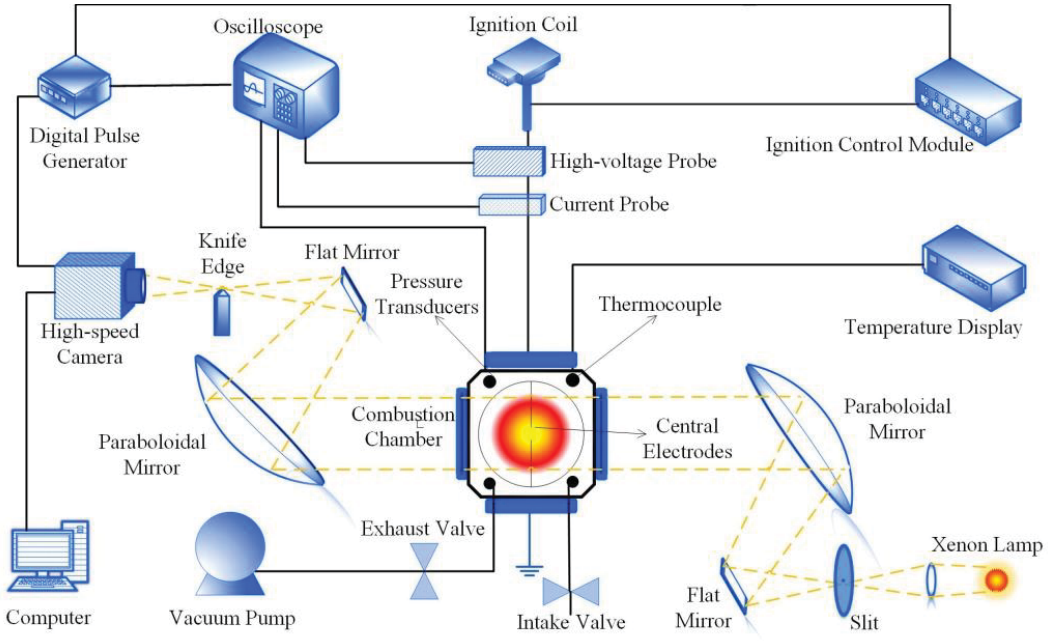

Fig. 1. Experimental setup

The combustion chamber of the CVCC has a capacity of 2.067 L, formed by the intersection of three orthogonal cylinders. There are two central electrodes for ignition. The vessel is also equipped with a K-type thermocouple (WRNK-231) and a pressure gauge (Keller LEX1) to monitor the initial temperature and pressure, and the piezoelectric pressure sensor (Kistler 6115A) and the charge amplifier (Kistler 5018A) are used to record the transient pressure signals during the explosion. The initial temperature is controlled by a Proportional Integral Derivative (PID) controller and heaters evenly arranged on each wall, which ensures a uniform temperature distribution inside the CVCC. Quartz windows are placed on both sides of the CVCC to provide an optical path for the Schlieren system so that the high-speed camera can record continuous flame images.

Table 1 shows the test matrix for this study. Experiments were conducted at $T_0 = 358, 418$ K, $P_0 =$

1-4 bar, O_2 = 21-25 % and ϕ = 0.7-1.4. The oxygen-enriched air used in the experiments is from a compressed cylinder supplied by xxx Company. The accuracy of the oxygen concentration is within ±0.01%. Before fuel injection, the combustion chamber is flushed with the oxygen-enriched air and then vacuumed to approximately 0.1 bar absolute pressure to ensure that water/ethanol evaporates rapidly. Then, fuel is injected into the chamber through a 500 μL micro syringe. The chamber was given at least 3 minutes for resting. Then, the air is introduced until the pressure in the chamber reaches the desired value, and a rest of at least 5 minutes to ensure the formation of homogeneous mixtures. The reference condition is set up at P_0 = 1 bar, T_0 = 358 K and O_2 = 23%. Compared with the reference condition, only one initial condition is changed at one time to investigate the influence of different initial conditions on explosion characteristics. Each case was repeated at least three times. The detailed description of the experimental setup and procedures has been given in previous publications [27-29].

Table 1. Test matrix

	Initial temperature (K)	Initial pressure (bar)	Oxygen concentration (%)	Equivalence ratio
Effect of initial temperature	358/388/418	1	23	0.7 – 1.4 with an interval of 0.1
Effect of initial pressure	358	1/2/4	23	
Effect of Oxygen concentration	358	1	21/23/25	

Some experiments at the boundary condition of ϕ=0.7 and T_0=358 K were not successful because the flame kernel failed to propagate further and it was extinct. Fig. 2 shows the flame images before they were extinct. This phenomenon can be attributed to the low laminar burning velocity and released heat which are not enough to sustain the flame.

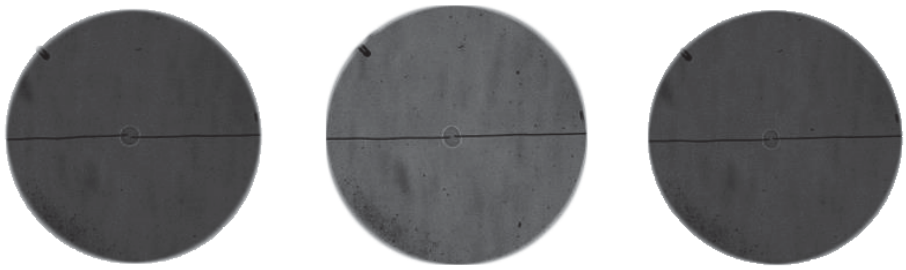

(a) O_2=21%, P_0=1 bar (b) O_2=23%, P_0=1 bar (c) O_2=25%, P_0=1 bar

Fig. 2. Flame images before extinction at ϕ=0.7 and T_0=358 K

3. Data evaluation

P_{max}, $(dP/dt)_{max}$, K_G and t_c are employed to evaluate the explosion characteristics of flammable mixtures. They provide critical information for understanding the explosion process, evaluating the safety of the combustion chamber and designing the explosion protection. These parameters are sensitive to initial conditions such as pressure, temperature, equivalence ratio, oxygen concentration and the composition of mixtures [19,30-32].

Fig. 3 shows the acquisition of the above explosion parameters. The raw pressure P has some oscillations caused by the channel effect of the pressure sensor. To eliminate this oscillation, a Gauss filter is used, and $P_{filtered}$ is obtained. Explosion parameters such as P_{max}, $(dP/dt)_{max}$ and t_c can be directly obtained from the pressure history after filtering. As shown in Fig. 3, P_{max} and $(dP/dt)_{max}$ are the maximum value of the pressure and the pressure rise rate curve, respectively. Combustion duration t_c

is defined as the time interval between ignition and peak pressure P_{max} [33,34].

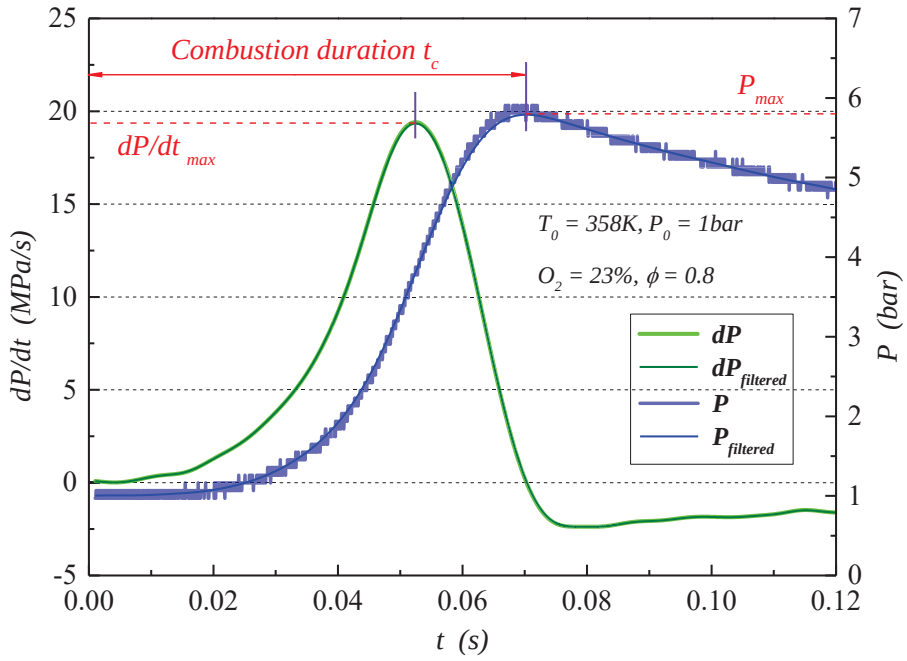

Fig. 3. Acquisition of explosion parameters

The hazards of explosion mainly depend on P_{max} and $(dP/dt)_{max}$, which are always affected by initial conditions as well as the shape and the size of combustion vessels. The deflagration index K_G is used for normalized the vessel size, which is defined as:

$$K_G = \left(\frac{dP}{dt}\right)_{\max} V^{1/3} \tag{1}$$

where V is the volume of vessels. This equation is generally used in spherical vessels or cylinder vessels with a length and diameter ratio lower than 2 [25]. For the present experiment, the combustion chamber is composed of three orthogonal cylinders and the overlapping part is almost spherical, complying with the requirements reported in NFPA 68 Standard [35]. The value of K_G reflects the explosion intensity of mixtures. Combustible mixtures can be categorized into three hazard classes. Table 2 lists hazard classes of deflagration.

Table 2. Hazard classes of deflagration [35]

Hazard Class	K_G ($MPa \cdot m/s$)
St-1	< 20
St-2	20-30
St-3	> 30

4. Results and discussion

4.1 Pressure evolution

Fig. 4 shows the histories of pressure at all test conditions. All curves exhibit a similar behaviour. The pressure increases slowly at the initial stage due to the limited heat release. Then, a rapid combustion stage starts where pressure rises drastically until it reaches to the maximum value. At the last stage, pressure drops gradually as the combustion reaches the end, because of the heat loss from the flame to the wall by radiation. Furthermore, at all conditions, the explosion pressure first rises with the increase of equivalence ratio and then drops slightly in the rich mixing ratio zone. The initial pressure has a greater effect on the explosion pressure than the initial temperature and the oxygen concentration. When the initial pressure gets higher, the explosion pressure is also proportionally increased. However, with the initial temperature decreasing or the oxygen concentration increasing, the explosion pressure increases slightly and the variation is within 1 bar.

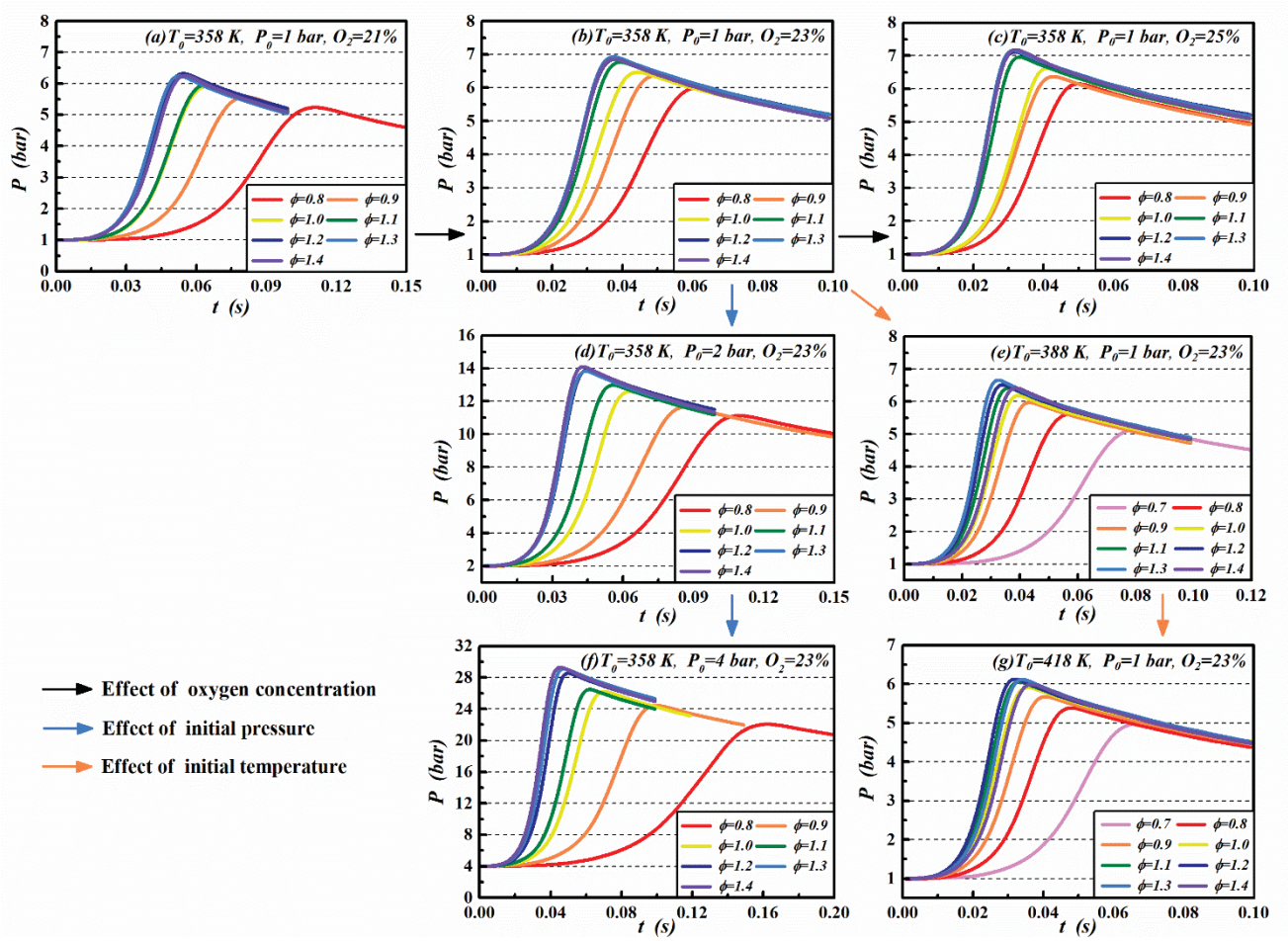

Fig. 4. Histories of pressure

Fig. 5 shows the histories of the pressure rise rate at all test conditions. The behaviour of pressure rise rates *dP/dt* is similar to that of pressures. *dP/dt* increases rapidly to the maximum and then drop immediately. Explosion pressure P_{max} is obtained when *dP/dt* reaches zero, and then *dP/dt* will continue to decrease and keep negative because of the heat loss to the chamber wall. In addition, the variation trend of $(dP/dt)_{max}$ versus equivalence ratio and initial conditions are also the same as those of P_{max}. The only difference is that $(dP/dt)_{max}$ hardly changes with the initial temperature, because of both P_{max} and t_c drop proportionally with the rise of initial temperature. The effects of different initial conditions on P_{max}, $(dP/dt)_{max}$ and K_G will be discussed in detail in the following sections.

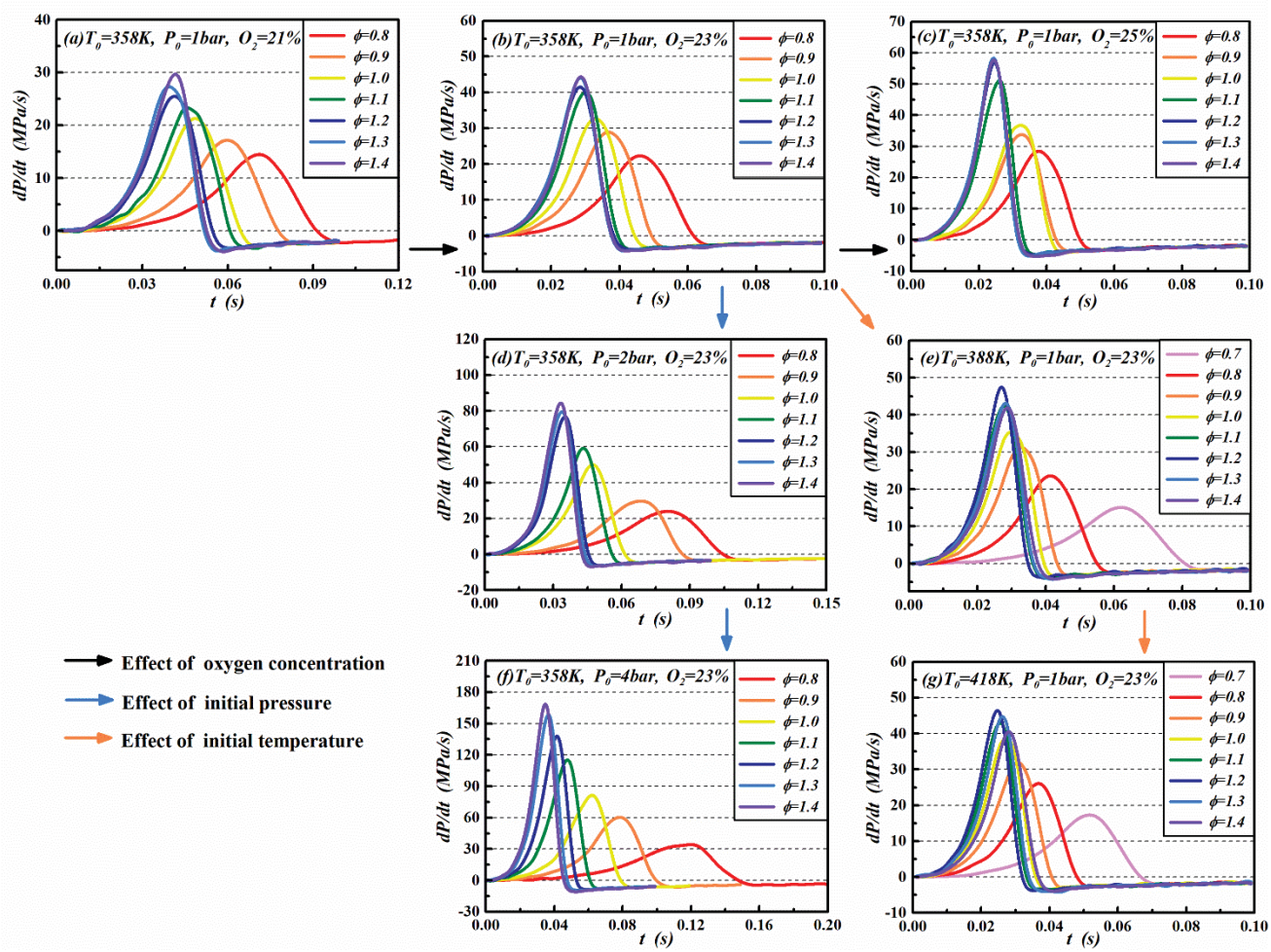

Fig. 5. Histories of pressure rise rate

4.2 Heat release

Heat release provides a quantitative basis for the analysis of the explosion parameter change. To simplify the calculation, the following assumptions are made [27]: (1) the mixed gas in the chamber is ideal gas; (2) the mixtures are evenly distributed and thermodynamic properties of mixtures are uniform; (3) the effects of combustion products are not considered. The authors acknowledge that errors will be introduced because of those assumptions. However, since all the calculations are made based on the same assumptions, the comparison of heat release results among different conditions is relatively fair.

Based on the above assumptions, the heat release in the chamber can be calculated as [36]:

$$\frac{dQ}{dt}=\left(\frac{1}{k_u-1}\right)V\frac{dP}{dt}+\left(\frac{k_u}{k_u-1}\right)P\frac{dV}{dt} \quad (2)$$

where Q, t, V, P, k_u stand for total released heat, time after ignition, volume of the chamber, pressure in the chamber and specific heat ratio, respectively. For this experiment in the CVCC, $dV = 0$. Then, the total heat release after combustion can be obtained by integrating Eq. (2) from $t = 0$ to $t = t_c$:

$$Q=\int_0^{t_c}\left(\frac{dQ}{dt}\right)dt \quad (3)$$

Fig. 6 shows the relationship between the net heat release of hydrous ethanol-air mixtures and equivalent ratios at all experimental conditions. Within the equivalent ratio of 0.7-1.1, the total heat release of combustible mixtures increases with the equivalent ratios due to the increase of fuel quantity. For mixtures with an equivalent ratio in the range of 1.2-1.4, there are different behaviours at different oxygen concentrations. Heat release obtains a higher value at a higher oxygen concentration but has little difference between ϕ = 1.2-1.4. For different initial temperature, heat release decreases with the increase of temperature, and it begins to drop from ϕ = 1.2-1.3 at the same temperature, probably because the mixtures do not burn completely. For different initial pressures, heat release is greatly affected due to more fuel is injected at a higher pressure. When the initial pressure P_0 increases form 1 bar to 4 bar at ϕ =1.0, heat release rises from 3.37 kJ to 11.31 kJ, which is less than the expected four-times relationship. Perhaps this is the result of an increase in heat loss. Based on the findings proposed by C. K. Law et al. [37], the increase of adiabatic flame temperature with P_0 is very small, meaning that the temperature difference between the flame front and the wall is almost constant. However, the density of unburned gas significantly increases with P_0, resulting in an obvious increase in the thermal conductivity, which leads to a higher heat loss at elevated pressures. Moreover, as the equivalent ratio increases, the marginal heat release gain is reduced and the heat release peaks at different equivalent

ratios for various P_0. This is because the heat loss at elevated pressures is large with respect to that at P_0 = 1 bar, and the adiabatic flame temperature gives the maximum at the rich end [37], meaning that the heat loss is larger at rich sides. Thus, the heat release is sensitive to heat loss for high pressures and rich mixtures, resulting in the change of the peak heat release position of equivalence ratio.

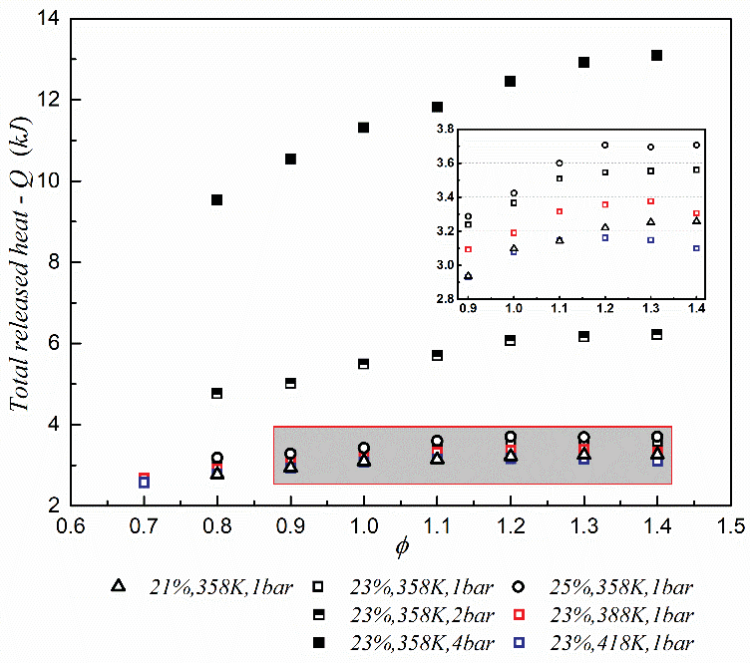

Fig. 6. Total released heat Q as the function of ϕ at all conditions

4.3 Effect of initial conditions on explosion parameters

4.3.1 Effect of equivalence ratio

Fig. 7 shows the maximum pressure P_{max} under all conditions. At 1 bar initial pressure, P_{max} varied less than 2 bar as the equivalence ratio rises from 0.8 to 1.4; however, as the initial pressure increases, the positive impact of initial pressure become more obvious. It is also found that the marginal P_{max} increase rate reduces with the equivalence ratio. Under the elevated oxygen concentration, P_{max} increases with the equivalence ratio. However, under the elevated initial temperature, P_{max} increases

first and it drops slightly at the rich conditions. For E80W20 tested in this study, P_{max} gives its peak value between ϕ = 1.2 and ϕ = 1.4.

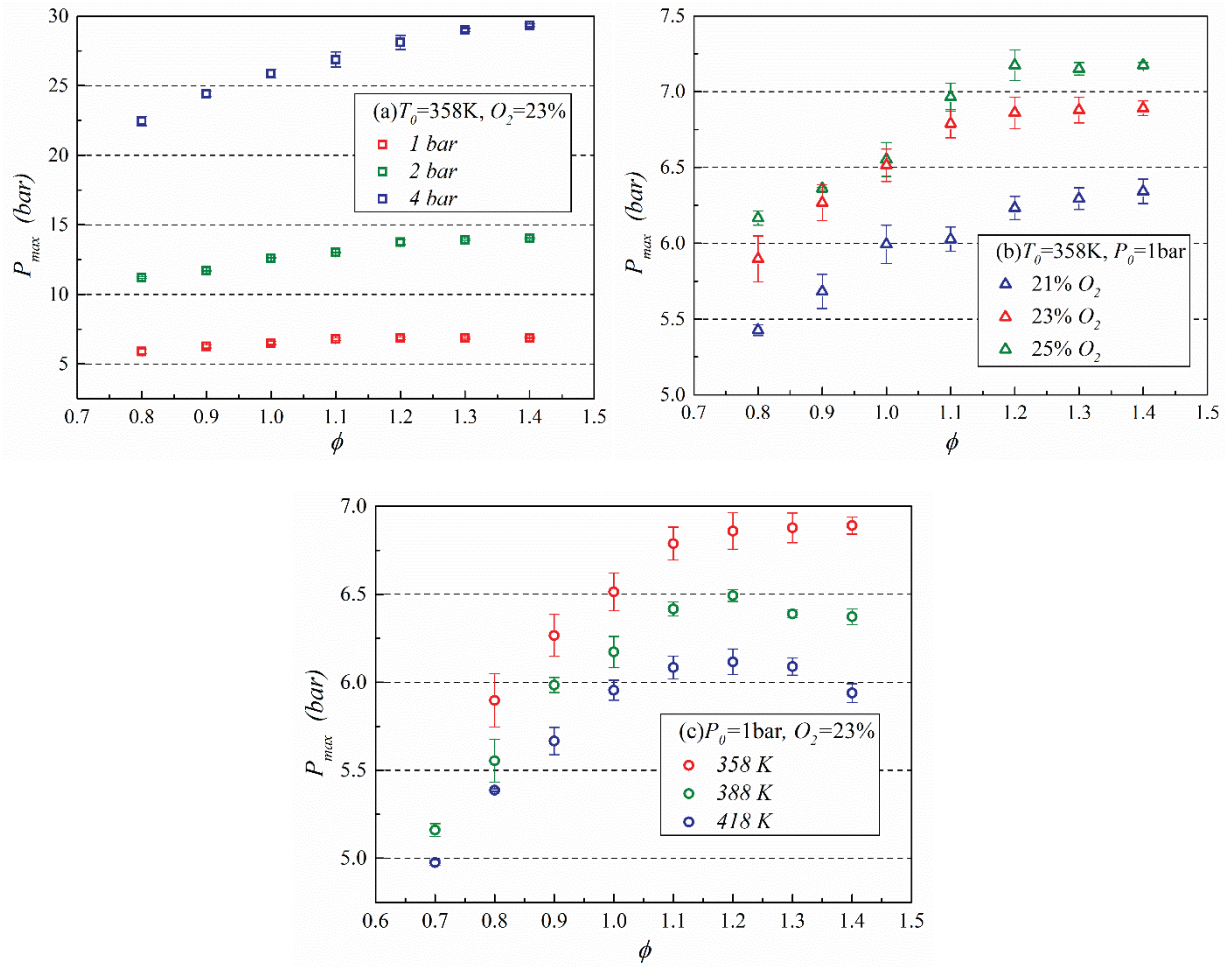

Fig. 7. P_{max} at different equivalence ratios

Fig. 8 presents the change of $(dP/dt)_{max}$ and K_G in wide equivalence ratios. Based on the definition (Eq.(1)) of K_G, K_G is proportional to $(dP/dt)_{max}$ since the chamber volume is costant, indicating that they have the same variation trend. Thus, K_G and $(dP/dt)_{max}$ are plotted into the same figure. As expected, the maximum rate of pressure rise increases with the equivalence ratio at T_0 = 358K. At different initial pressures, the maximum rate of pressure rise for lean hydrous ethanol-air mixtures are similar, but the difference is gradually amplified as the equivalence ratio gets higher. Moreover, the peak appears at different equivalence ratios for various P_0 because of the flame instability. As shown

in Fig. 9, for rich mixtures, the flame is easier to be cellular and instable, which will cause the large pressure fluctuations and promote further increase of $(dP/dt)_{max}$ even if there is no oxygen for combustion. Within the investigated temperature range, the maximum rate of pressure rise is insensitive to the temperature variation, which agrees with the findings from Mitu [24]. There are two opposite effects working together to cause this behaviour. On the one hand, the increase of T_0 results in a visible diminution of explosion pressure, as shown in Fig. 7. On the other hand, the research reported by Hinton et al. [15] and Liang et al. [38] indicate that the laminar burning velocity of hydrous ethanol increases with T_0, resulting in a shorter combustion duration, which offsets the negative impact of the decrease of explosion pressure on $(dP/dt)_{max}$. Similar to the explosion pressure, as T_0 increases, $(dP/dt)_{max}$ decreases slightly at the rich mixtures, and the peak position gradually shifts to the left, from ϕ = 1.4 at 358 K to ϕ = 1.2 at 418 K.

Deflagration index K_G strongly depends on P_0 and ϕ. It is clearly seen that K_G multiplies at the high pressure and equivalence ratio. When P_0 = 4 bar and ϕ = 1.3 or 1.4, K_G gives a higher value, but for other conditions, K_G is all lower than 20 MPa·m/s, indicating that E80W20 belongs to the hazard class *St 1*.

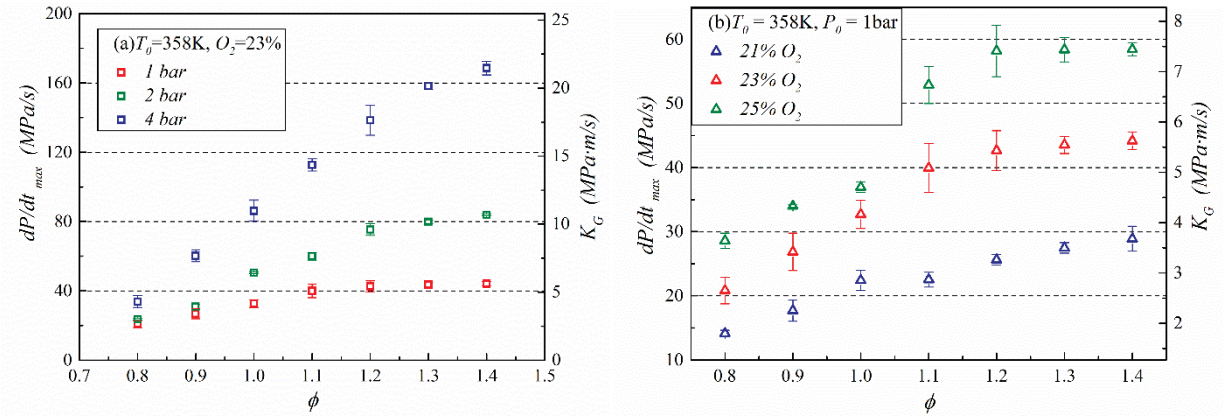

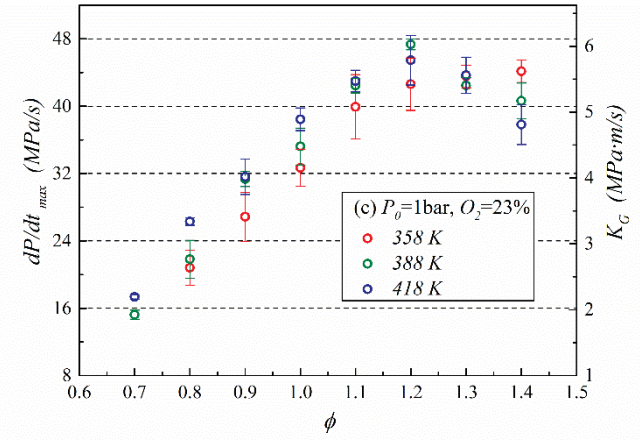

Fig. 8. $(dP/dt)_{max}$ and K_G at different equivalence ratios

(a) P_0=1 bar (b) P_0=2 bar (c) P_0=4 bar

Fig. 9. Flame instability images at ϕ=1.3, T_0=358 K and O_2=23%

Fig. 10 shows the combustion duration t_c at all initial conditions. With the rise of equivalence ratio, t_c first significantly decreases until the equivalence ratio of approximately 1.1, and then it becomes flat or even increases slightly. Regardless of the initial pressure and oxygen concentration, t_c gives the minimum value at ϕ = 1.2-1.3, but the peak position will shift left a little with the initial temperature getting higher, which is consistent with the phenomenon found in the explosion pressure and the maximum rate of pressure rise. At ϕ = 1.2-1.3, the combustion is the quickest, which is different from the widely accepted finding that the fastest combustion velocity usually happens at approximately ϕ =1.1. Reasoning with C. K. Law's paper [37], perhaps this could be as a consequence of extreme

dissociation on the lean side, so that the heat release peaks on the rich side. Hence, combustion can peak at ϕ =1.1, 1.2 and most likely 1.3. Although, most papers normally show the peak at ϕ =1.1, there some papers which obtained the peak at richer sides. For instance, Zhang et al. [39] found that the laminar burning velocity of 75 vol% hydrous ethanol with different hydrogen addition (0-80% mole fraction relative to the fuel) always reached the maximum value at ϕ =1.2. Bradley et al. [40] obtained the largest mass burning velocity of *i*-octance/air mixtures at ϕ =1.3 and Bao et al. [41] got the largest laminar burning velocity of cyclopentanone at ϕ =1.2 for various temperatures. In addition, due to the large quantity of water, the combustion reactions might be affected, leading to the fastest combustion velocity moving from 1.1 to 1.2 or 1.3. More chemical kinetic mechanism investigations are needed to confirm this.

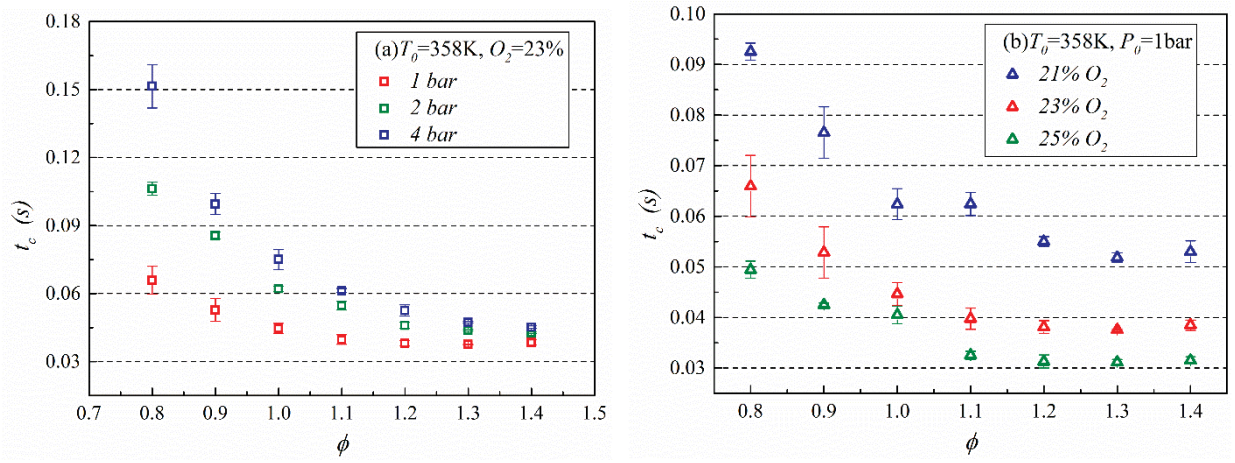

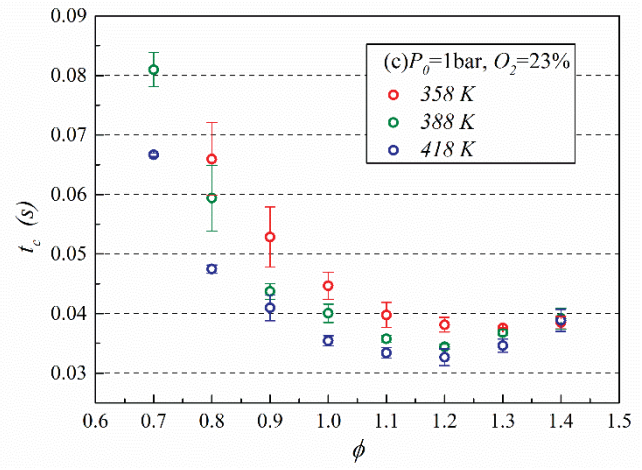

Fig. 10. t_c at all initial conditions

4.3.2 Effect of initial pressure

Fig. 11 displays the impact of initial pressure on P_{max}, $(dP/dt)_{max}$, K_G and t_c under the conditions of T_0 = 358 K and O_2 = 23%. P_{max} is a linear function of P_0 for all equivalence ratios (R^2 of linear correlation > 0.99). The following equation shows the linear relationship.

$$P_{\max} = a + bP_0 \tag{4}$$

Both a and b are positive, indicating that P_{max} monotonically increases with P_0, mainly because the mass of combustible mixtures increases linearly with P_0 when other initial parameters are kept constant. In addition, as the equivalence ratio gets higher, the slope of fitting lines b rises slightly. The maximum b (7.506) is obtained at ϕ = 1.4.

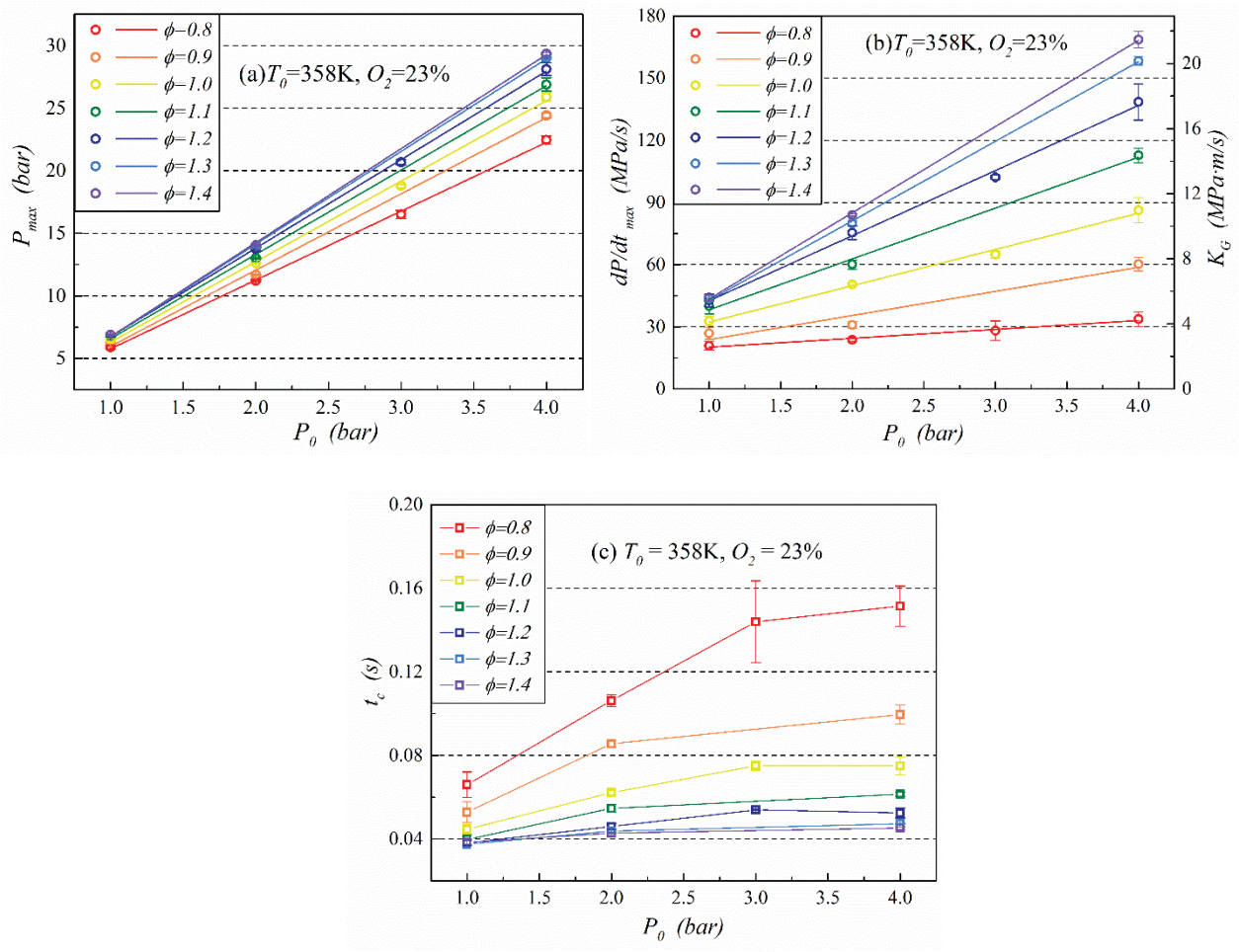

Fig. 11. P_{max}, $(dP/dt)_{max}$, K_G and t_c versus P_0 at different equivalent ratios

$(dP/dt)_{max}$ and K_G are also linear functions of P_0 (R^2 of linear correlation > 0.97). The following equation shows the linear relationship.

$$(dP/dt)_{max} = c + dP_0 \tag{5}$$

$$K_G = e + kP_0 \tag{6}$$

where coefficients d and k stand for the sensitivity of $(dP/dt)_{max}$ and K_G to the initial pressure variation, respectively. All coefficients in the Eq. (5) and (6) are positive, meaning that both $(dP/dt)_{max}$ and K_G increase with P_0. Moreover, slopes d and k increase with ϕ, revealing that the explosion hazard becomes more sensitive to the initial pressure for rich fuel-air mixtures. The explosion risk is higher at rich mixture and high initial pressure.

Table 3 summaries the slopes of fitting lines with initial pressure for P_{max}, $(dP/dt)_{max}$ and K_G at different equivalence ratios. Similar results were found for other combustible fuels, such as pentanol [42], propane [43] and ethylene [44].

Table 3. Slopes of fitting lines with initial pressure for P_{max}, $(dP/dt)_{max}$ and K_G

ϕ	0.8	0.9	1.0	1.1	1.2	1.3	1.4
b	5.495	6.087	6.429	6.732	7.067	7.399	7.506
d	4.294	11.619	17.509	24.557	31.441	38.376	41.594
k	0.547	1.480	2.230	3.128	4.005	4.889	5.298

The combustion duration t_c increases with the initial pressure, especially at lean conditions, resulting from the decrease in the laminar burning velocity. But the variation in combustion duration is not strictly linear and it is strongly affected by the equivalence ratios. When P_0 increases from 1 bar to 4 bar, t_c is increased from 66 ms to 151 ms at ϕ = 0.8. However, at ϕ = 1.4, there is only a 9 ms increase from 38 ms (1 bar initial pressure) to 47 ms (4 bar initial pressure), which means that the effect of P_0 on the combustion duration is small enough to be ignored for rich fuel-air mixtures.

4.3.3 Effect of initial temperature

Fig. 12 shows the impact of initial temperature on P_{max}, $(dP/dt)_{max}$, K_G and t_c under conditions of $P_0 = 1bar$ and $O_2 = 23\%$. The decrease of initial temperature results in higher explosion pressure. This is because when P_0 and the volume of the chamber remain constant, the density of the combustible mixture inside the chamber decreases with the increase of T_0, which lowers the heat release and delivers a diminution in explosion pressure. Furthermore, slopes for all equivalence ratios except ϕ = 1.4 are nearly equal, indicating that the explosion pressure has the same sensitivity to initial temperature.

The variation of $(dP/dt)_{max}$ with initial temperature is more complex. As described in the subsection *4.3.1*, $(dP/dt)_{max}$ is insensitive to the temperature variation, the values of $(dP/dt)_{max}$ between three temperatures are close at the same equivalent ratio, but there still is a slight difference. With the increase of T_0, P_{max} decreases but the laminar burning velocity increases, the common result of these two opposite effects is: when the equivalence ratio is lower than 1.1, $(dP/dt)_{max}$ increases slightly with T_0, that is, the decrease of explosion pressure is insufficient to offset the increase of the laminar burning velocity; when the equivalence ratio is higher than 1.1, the situation gradually reverses, reflected on the figure as $(dP/dt)_{max}$ decreases with T_0.

With the increase of T_0, the combustion duration roughly decreases because of increased the laminar burning velocity. Moreover, the influence of T_0 is dependent on the equivalence ratio. There is a significant reduction in combustion duration at $\phi = 0.8$. However, for rich fuel-air mixtures, the effect of initial temperature is not obvious. There is only a 2 ms acceleration from 38.5 ms to 36.5 ms at $\phi = 1.4$ when T_0 increases from 358 K to 418 K.

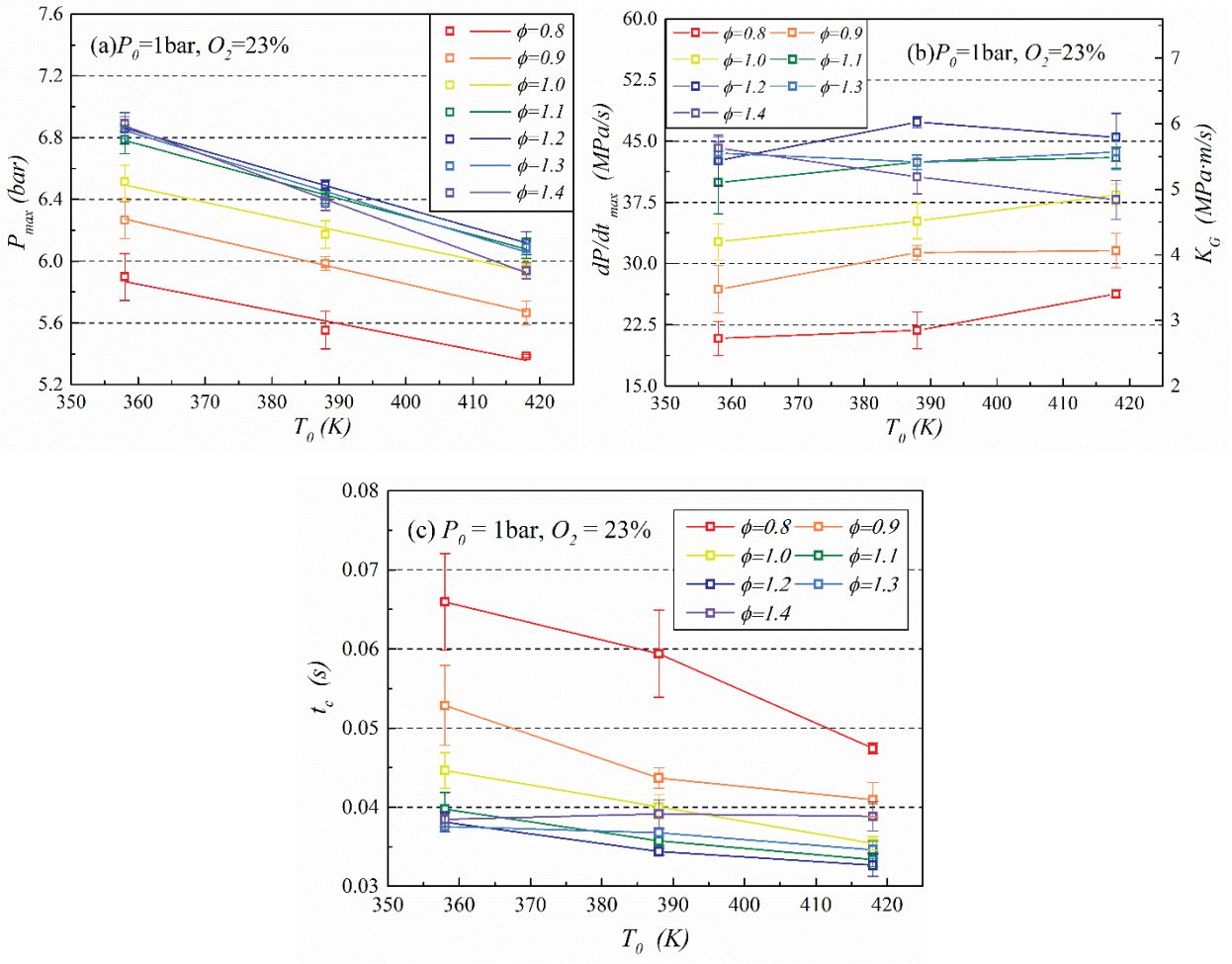

Fig. 12. P_{max}, $(dP/dt)_{max}$, K_G and t_c versus initial temperature T_0 at different equivalent ratios

4.3.4 Effect of oxygen concentration

Fig. 13 shows the impact of initial oxygen concentration on P_{max}, $(dP/dt)_{max}$, K_G and t_c under the conditions of T_0 = 358K and P_0 = 1bar. With the increase of the initial oxygen concentration, P_{max} visibly increases. But at the same equivalent ratio, especially around ϕ = 1.0, P_{max} at the initial oxygen concentration of 23% is not equal to the average value of P_{max} at 21% and 25% O_2, and it is closer to that of 25% O_2. This shows that that the positive effect of oxygen on the combustion reaction does not increase linearly with the oxygen concentration. $(dP/dt)_{max}$ increases proportionally with the increase of oxygen concentration, which means that the combustion is more intense at higher oxygen

concentration, resulting in a stronger explosion.

With the increase of oxygen concentration, the combustion duration has a visible decrease, meaning that enhancing oxygen concentration is an effective way to shorten the combustion duration, especially for lean fuel-air mixtures. However, the change is not linear but gradually decreases with the increase of the oxygen concentration.

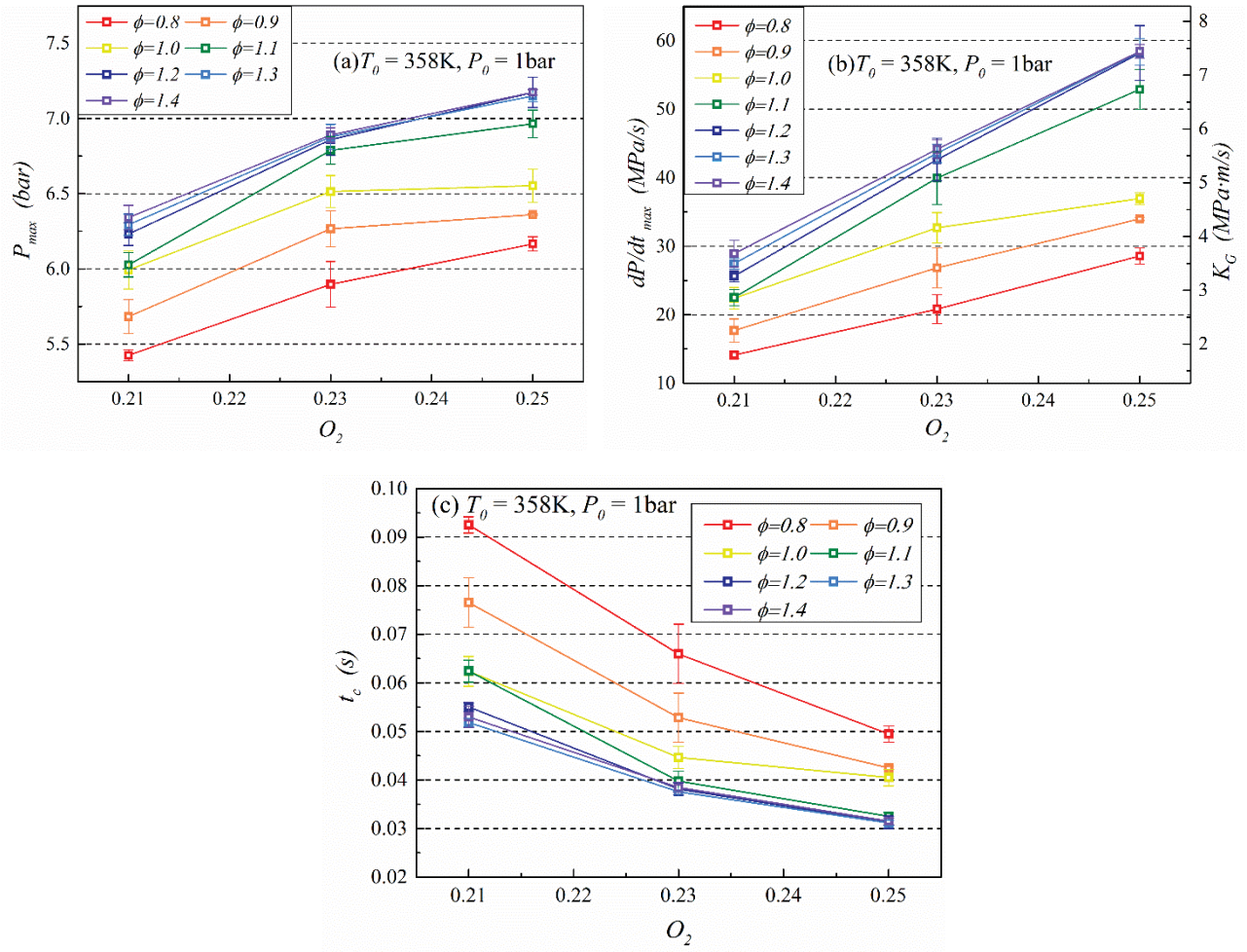

Fig. 13. P_{max}, $(dP/dt)_{max}$, K_G and t_c versus oxygen concentration at $T_0 = 358K$ and $P_0 = 1bar$

5. Conclusion

A study was conducted in a CVCC to investigate the explosion characteristics of hydrous bio-ethanol containing 20 vol% water (E80W20). The test boundary conditions are P_0 = 1.4 bar, T_0 = 358

418 K, O_2 = 21%-25% and ϕ = 0.7-1.4. Explosion parameters such as explosion pressure P_{max}, maximum rate of pressure rise $(dP/dt)_{max}$, deflagration index K_G and combustion duration t_c were calculated and discussed. It was found that P_{max} and $(dP/dt)_{max}$ increase linearly with the initial pressure. P_{max} decreases linearly with the initial temperature, but $(dP/dt)_{max}$ did not change. P_{max} increases with the oxygen concentration, however, the increase rate reduces at a higher oxygen concentration. $(dP/dt)_{max}$ linearly increases with the oxygen concentration. t_c decreases first and then increases with the increase of equivalence ratios, and it reaches the minimum at ϕ = *1.2-1.3*, which is independent of initial pressure and oxygen concentration. With the decrease of initial pressure or the increase of initial temperature and oxygen concentration, t_c is shortened; however, for rich fuel-air mixtures, it varies little with the above initial conditions. For most initial conditions investigated in this paper, K_G is lower than 20 MPa·m/s, revealing that E80W20 is relatively safe when it is combusted with air with a 23% oxygen content.

Acknowledgements

The work is supported by the Open Project of State Key Laboratory of Automotive Safety and Energy (NO. KF1817), the National Key R&D Program of China (2018YFB1501405), the National Natural Science Foundation of China (NO.91741203), and the Hangzhou Science Committee (NO.20162013A06) of China.

References:

[1] Johnson T, Joshi A. Review of Vehicle Engine Efficiency and Emissions. SAE Int J Engines 2018;11(6):1307-30.
[2] Lanzanova TDM, Dalla Nora M, Zhao H. Performance and economic analysis of a direct injection spark ignition engine fueled with wet ethanol. Appl Energ 2016;169:230-9.
[3] Munsin R, Laoonual Y, Jugjai S, Imai Y. An experimental study on performance and emissions of a small SI engine generator set fuelled by hydrous ethanol with high water contents up to 40%. Fuel 2013;106:586-92.
[4] Wang C, Herreros JM, Jiang C, Sahu A, Xu H. Engine Thermal Efficiency Gain and WTW GHG Savings when using Bioethanol as a Gasoline-Blending Component in Future SI engine: A China Case Study. Energ Fuel 2018;32(2):1724-32.
[5] Xu H, Wang C, Ma X, Sarangi AK, Weall A, Krueger-Venus J. Fuel injector deposits in direct-injection spark-ignition engines. Prog Energ Combust 2015;50:63-80.
[6] Wang C, Xu H, Herreros JM, Wang J, Cracknell R. Impact of fuel and injection system on particle emissions from a GDI engine. Appl Energ 2014;132:178-91.
[7] Wang C, Xu H, Herreros JM, Lattimore T, Shuai S. Fuel Effect on Particulate Matter Composition and Soot Oxidation in a Direct-Injection Spark Ignition (DISI) Engine. Energ Fuel 2014;28(3):2003-12.
[8] Wang C, Janssen A, Prakash A, Cracknell R, Xu H. Splash blended ethanol in a spark ignition engine – Effect of RON, octane sensitivity and charge cooling. Fuel 2017;196:21-31.
[9] Wang C, Prakash A, Aradi A, Cracknell R, Xu H. Significance of RON and MON to a modern DISI engine. Fuel 2017;209:172-83.
[10] Wang C, Zeraati-Rezaei S, Xiang L, Xu H. Ethanol blends in spark ignition engines: RON, octane-added value, cooling effect, compression ratio, and potential engine efficiency gain. Appl Energ 2017;191:603-19.
[11] Saxena S, Schneider S, Aceves S, Dibble R. Wet ethanol in HCCI engines with exhaust heat recovery to improve the energy balance of ethanol fuels. Appl Energ 2012;98:448-57.
[12] Flowers DL, Aceves SM, Frias JM. Improving Ethanol Life Cycle Energy Efficiency by Direct Utilization of Wet Ethanol in HCCI Engines. J Energ Resour-Asme 2007;129(4):332-7.
[13] Khaliq A, Trivedi SK, Dincer I. Investigation of a wet ethanol operated HCCI engine based on first and second law analyses. Appl Therm Eng 2011;31(10):1621-9.
[14] Mack JH, Aceves SM, Dibble RW. Demonstrating direct use of wet ethanol in a homogeneous charge compression ignition (HCCI) engine. Energy 2009;34(6):782-7.
[15] Hinton N, Stone R, Cracknell R, Olm C. Aqueous ethanol laminar burning velocity measurements using constant volume bomb methods. Fuel 2018;214:127-34.
[16] Lanzanova TDM, Dalla Nora M, Martins MES, Machado PRM, Pedrozo VB, Zhao H. The effects of residual gas trapping on part load performance and emissions of a spark ignition direct injection engine fuelled with wet ethanol. Appl Energ 2019;253:113508.
[17] Salzano E, Basco A, Cammarota F, Di Sarli V, Di Benedetto A. Explosions of syngas/CO 2 mixtures in oxygen-enriched air. Ind Eng Chem Res 2012;51:7671-8.
[18] Nauclér JD, Christensen M, Nilsson EJK, Konnov AA. Oxy-fuel Combustion of Ethanol in Premixed Flames. Energ Fuel 2012;26(7):4269-76.
[19] Chang YM, Lee JC, Chen CC, Shu CM. Fire and explosion properties examinations of toluene – methanol mixtures approached to the minimum oxygen concentration. J Therm Anal Calorim 2009;96(3):741-9.
[20] BS EN 1839-2017. 2017;
[21] De Smedt G, de Corte F, Notele R, Berghmans J. Comparison of two standard test methods for determining explosion limits of gases at atmospheric conditions. J Hazard Mater 1999;70(3):105-13.
[22] Rahman KM, Kawahara N, Tsuboi K, Tomita E. Combustion characteristics of wet ethanol ignited using a focused Q-switched Nd:YAG nanosecond laser. Fuel 2016;165:331-40.
[23] Yi F. Oxy-combustion of high water content fuels. Dissertations & Theses - Gradworks 2013;

[24] Mitu M, Brandes E. Influence of pressure, temperature and vessel volume on explosion characteristics of ethanol/air mixtures in closed spherical vessels. Fuel 2017;203:460-8.
[25] Li Q, Cheng Y, Huang Z. Comparative assessment of the explosion characteristics of alcohol – air mixtures. J Loss Prevent Proc 2015;37:91-100.
[26] Mitu M, Brandes E, Hirsch W. Mitigation effects on the explosion safety characteristic data of ethanol/air mixtures in closed vessel. Process Saf Environ 2018;117:190-9.
[27] Xu C, Fang D, Luo Q, Ma J, Xie Y, Zheng X. Characterization of gasoline combustion with laser and spark ignition. J Zhejiang Univ-Sc A 2015;16(10):830-8.
[28] Xu C, Zhou K, Li X, Zhong A, Oppong F, Wang H, et al. Laminar Burning Characteristics of Two Rice-Husk-Derived Biofuels. Energ Fuel 2018;32(9):9872-82.
[29] Xu C, Zhong A, Li X, Wang C, Sahu A, Xu H, et al. Laminar burning characteristics of upgraded biomass pyrolysis fuel derived from rice husk at elevated pressures and temperatures. Fuel 2017;210:249-61.
[30] Tang C, Zhang S, Si Z, Huang Z, Zhang K, Jin Z. High methane natural gas/air explosion characteristics in confined vessel. J Hazard Mater 2014;278:520-8.
[31] Tang C, Huang Z, Jin C, He J, Wang J, Wang X, et al. Explosion characteristics of hydrogen – nitrogen – air mixtures at elevated pressures and temperatures. Int J Hydrogen Energ 2009;34(1):554-61.
[32] Mitu M, Brandes E. Explosion parameters of methanol – air mixtures. Fuel 2015;158:217-23.
[33] Zhang B, Xiu G, Bai C. Explosion characteristics of argon/nitrogen diluted natural gas – air mixtures. Fuel 2014;124:125-32.
[34] Cui G, Wang S, Liu J, Bi Z, Li Z. Explosion characteristics of a methane/air mixture at low initial temperatures. Fuel 2018;234:886-93.
[35] Association NFP. NFPA 68_Guide for Venting of Deflagrations. 2002;
[36] Sorapipatana C, Yoosin S. Life cycle cost of ethanol production from cassava in Thailand. Renew Sust Energ Rev 2011;15(2):1343-9.
[37] Law C, Makino A, Lu T. On the off-stoichiometric peaking of adiabatic flame temperature. Combust Flame 2006;145(4):808-19.
[38] Liang K, Stone R. Laminar burning velocity measurement of hydrous methanol at elevated temperatures and pressures. Fuel 2017;204:206-13.
[39] Zhang Z, Li G, Ouyang L, Pan Z, You F, Gao X. Experimental determination of laminar burning velocities and Markstein lengths for 75% hydrous-ethanol, hydrogen and air gaseous mixtures. Int J Hydrogen Energ 2011;36(20):13194-206.
[40] Bradley D, Lawes M, Liao S, Saat A. Laminar mass burning and entrainment velocities and flame instabilities of i-octane, ethanol and hydrous ethanol/air aerosols. Combust Flame 2014;161(6):1620-32.
[41] Bao X, Jiang Y, Xu H, Wang C, Lattimore T, Tang L. Laminar flame characteristics of cyclopentanone at elevated temperatures. Appl Energ 2017;195:671-80.
[42] Li Q, Cheng Y, Jin W, Huang Z. Comparative study on the explosion characteristics of pentanol isomer – air mixtures. Fuel 2015;161:78-86.
[43] Razus D, Brinzea V, Mitu M, Movileanu C, Oancea D. Temperature and pressure influence on maximum rates of pressure rise during explosions of propane – air mixtures in a spherical vessel. J Hazard Mater 2011;190(1-3):891-6.
[44] Movileanu C, Razus D, Oancea D. Additive effects on the rate of pressure rise for ethylene – air deflagrations in closed vessels. Fuel 2013;111:194-200.

当前使用的样式是 [Fuel_]

当前文档包含的题录共56条

有0条题录存在必填字段内容缺失的问题

所有题录的数据正常